Mechanism of SiN etching rate fluctuation in atomic layer etching

Cite as: J. Vac. Sci. Technol. A **38**, 062601 (2020); https://doi.org/10.1116/6.0000257
Submitted: 14 April 2020 . Accepted: 08 September 2020 . Published Online: 09 November 2020

Akiko Hirata, Masanaga Fukasawa, Katsuhisa Kugimiya, Kojiro Nagaoka, Kazuhiro Karahashi, Satoshi Hamaguchi, and Hayato Iwamoto

JVST A
Journal of Vacuum Science & Technology A

ARTICLE

avs.scitation.org/journal/jva

Mechanism of SiN etching rate fluctuation in atomic layer etching[a)]

Cite as: J. Vac. Sci. Technol. A 38, 062601 (2020); doi: 10.1116/6.0000257
Submitted: 14 April 2020 · Accepted: 8 September 2020 ·
Published Online: 9 November 2020

Akiko Hirata,[1,2,b)] Masanaga Fukasawa,[1] Katsuhisa Kugimiya,[1] Kojiro Nagaoka,[1] Kazuhiro Karahashi,[2] Satoshi Hamaguchi,[2] and Hayato Iwamoto[1]

AFFILIATIONS

[1]Research Division 2, Sony Semiconductor Solutions Corporation., 4-14-1 Asahi-cho, Atsugi, Kanagawa 243-0014, Japan
[2]Center for Atomic and Molecular Technologies, Osaka University, 2-1 Yamadaoka, Suita, Osaka 565-0871, Japan

Note: This paper is part of the Special Topic Collection Commemorating the Career of John Coburn.
[a)]This article is based on material presented at the 66th Symposium of the American Vacuum Society.
[b)]**Electronic mail:** Akiko.Hirata@sony.com

ABSTRACT

Atomic layer etching (ALE) enables atomic-precision control of the surface reaction for device fabrication. In this study, we investigate SiN ALE with process optimization of the surface adsorption and desorption steps, and we clarify the rate fluctuation mechanism. When we attempted CH_3F/Ar plasma adsorption followed by the subsequent Ar desorption step, an etch stop was observed owing to the excess deposition (>6 nm) of a protective film on the surface. X-ray photoelectron spectroscopy analysis revealed that a high number of C–C bonds was detected. As the bonding energy of C–C (6.4 eV) is high, these bonds remain after the desorption step. The excess C-rich polymer deposition after ALE originates from the residual C–C bonds. To suppress the C-rich polymer deposition, we studied stable SiN ALE using a desorption step with Ar/O_2 plasma (0.36 nm/cycle) and a two-step sequential desorption with Ar and O_2 plasma (0.6 nm/cycle), which resulted in stable SiN ALE processes. Because the surface condition is able to fluctuate with the number of cycles, precise surface control is strongly required to achieve stable ALE. Control of the plasma–wall interaction is also important for stable SiN ALE. We intentionally changed the chamber wall conditions and found that the polymer-deposited wall caused a fluctuation of the etched amount, which resulted from CF_x desorption from the deposited polymer. Thus, it is also important to control the influence of desorbed species from the chamber components for suppression of the ALE fluctuation.

I. INTRODUCTION

The size of semiconductor devices is continuously being scaled down, and there is a demand for the precise control of the etched profiles and a minimization of damage during dry etching. Atomic layer etching (ALE) is a promising technology that is able to overcome these issues.[1–3] ALE has been widely developed in recent years with an emphasis on Si-based,[4] dielectric-based,[5–15] and metal-based[16–19] materials processing. In this paper, we focus on ALE for dielectric films, which consists of two sequential steps: the surface adsorption of a polymer and desorption steps. The desorption step can be classified into three categories that are based on chemical, physical, and thermal desorption. To realize anisotropic etched profiles, the physical desorption by Ar plasma is discussed.

ALE for dielectric films has been developed mainly for SiO_2.[5–9] One of the applications of SiO_2 ALE is for high-aspect-ratio self-aligned contacts (SAC). As SiO_2 ALE has a higher selectivity of SiO_2 over SiN, compared with conventional continuous wave (CW) etching, better SAC profiles can be obtained.[9] SiO_2 ALE has been applied to advanced logic devices for the sub-7-nm technology generation. In the SiO_2 ALE process, a fluorocarbon polymer is adsorbed by C_4F_8/Ar plasma, followed by the subsequent physical desorption by Ar plasma. During desorption, by-products such as SiF_x and CO_x are generated. In the case of adsorption with C_4F_8/Ar plasma, a thick polymer is deposited on the mask and underlying materials (i.e., SiN and Si). Thus, highly selective SiO_2 etching can be performed.

SiN is also widely used in device structures, such as in the sidewall of transistor gates and the liner-layer at the contact

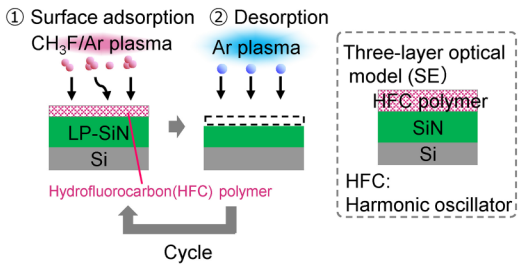

FIG. 1. Schematic of SiN ALE sequence and optical model for spectroscopic ellipsometry.

bottom. However, the number of published papers related to SiN ALE is much lower than that related to SiO_2 ALE. Thus, we investigated the SiN ALE in detail. There are two main proposed methods of SiN ALE. The first consists of two steps: modified layer generation by H_2 plasma and then removal of the modified layer.[13–15] However, H_x^+ ions penetrate deep into the surface even at a low energy. Thus, the H_x^+ ions may cause damage to the underlying layer in device fabrication. The other is a method in which a hydrofluorocarbon (HFC) polymer is adsorbed by CH_3F/Ar plasma and the reactive layer is desorbed by Ar plasma.[10–12] We focus on the latter method since less damage is expected.

To date, most of the reports on SiN ALE have focused on the mechanism, and few reports have been published that discuss the issues encountered in device fabrication. However, when ALE is used for device manufacturing, process stability and suppression of fluctuation, which depend on the chamber conditions, are extremely important.[20,21] Therefore, we investigate SiN ALE stability with process optimization of the surface adsorption and desorption steps, and we clarify the rate fluctuation mechanism.

II. EXPERIMENT

A dual frequency capacitively coupled plasma reactor (60 MHz/2 MHz) was used in this study. SiN (50 nm) was deposited on the Si substrate by low pressure chemical vapor deposition. One etching cycle consisted of two steps. CH_3F/Ar plasma was applied to deposit the HFC polymer as the adsorption step. The bias power was 0 W. The gas flow rates of CH_3F and Ar were 40 and 460 SCCM, respectively. Then, Ar plasma was used in the desorption step. The peak-to-peak voltage (V_{pp}) of the bottom electrode was 330 V in the desorption. The high energy peak of simulated ion energy distribution function for the Ar desorption step was nearly equal to the V_{pp}. By repeating this sequence, SiN ALE was achieved (Fig. 1). The conditions for each experiment are shown in Tables I and II. The thicknesses of SiN and the HFC polymer were measured by spectroscopic ellipsometry (SE), XPS, and transmission electron microscopy (TEM). The optical constants of the HFC polymer were determined by SE. Fitting was performed using an HFC polymer with a thickness of approximately 6 nm. A three-layer optical model (HFC polymer/SiN/Si) with fixed optical constants was used for the analysis of the thicknesses. The chemical bonding of the SiN surface was analyzed by XPS. The measurement was carried out on a PHI Quantera II system using a monochromatic Al source ($h\nu = 1486.6$ eV).

To study the interaction between the plasma and the wall surfaces, which affects the ALE stability, the chamber wall conditions were intentionally varied.[20,21] As a pretreatment, cleaning was performed with O_2 plasma for 300 s. After that, irradiation with C_4F_8/Ar plasma was performed for 0, 90, and 180 s to deposit the polymer on the chamber wall. Thereafter, SiN ALE was performed to evaluate the etching rate uniformity. As the chamber wall condition will cause a C/F density fluctuation in the plasma, the effect of the plasma–wall interactions can be analyzed.

The transition time between each step is also important to evaluate the C/F density fluctuation in the adsorption and desorption steps. To study the effect of residual gas in the previous step, ALE was performed by changing the gas transition time between the adsorption and desorption steps. After O_2 plasma cleaning as a pretreatment, we set the CH_3F/Ar gas flow for 20 s as the gas flow stabilization step. CH_3F/Ar plasma were irradiated for 4 s as the adsorption step. Then, as the gas transition step, Ar gas was flowed for 20 or 1 s. In the following desorption step, Ar plasma was irradiated for 60 s, and finally O_2 flash was performed to evaluate the etching rate uniformity.

There are no error bars in the graphs due to insufficient data point. However, all of experiments were performed in the mass production tool that is strictly controlled to keep the sufficient

TABLE I. Experiment.

Experiment	Adsorption				Transition Time (s)
	Pressure (mTorr)	Gas flow rate (SCCM)	Ion energy (eV)	Time (s)	
(a) Adsorption	40	CH_3F/Ar = 40/460	~25	4, 8, 12	
(b) Adsorption	40	CH_3F/Ar = 15/485	~25	4, 8, 12	
(c) ALE	40	CH_3F/Ar = 15/485	~25	4	20
(d) ALE w/O_2 desorption	40	CH_3F/Ar = 15/485	~25	4	20
(e) ALE w/O_2 ashing	40	CH_3F/Ar = 15/485	~25	4	20
(f) ALE (plasma–wall interaction)	40	CH_3F/Ar = 15/485	~25	4	20
(g) ALE (gas transition study)	40	CH_3F/Ar = 15/485	~25	4	1, 20

TABLE II. Experiment.

	Desorption				O_2 ashing				
Experiment	Pressure (mTorr)	Gas flow rate (SCCM)	Ion energy (eV)	Time (s)	Pressure (mTorr)	Gas flow rate (SCCM)	Ion energy (eV)	Time (s)	Cycle No.
(a) Adsorption									1
(b) Adsorption									1
(c) ALE	40	Ar = 500	330	10					1, 2, 3, 5, 10
(d) ALE w/O_2 desorption	40	O_2/Ar = 50/450	300	60					1, 5, 8, 10
(e) ALE w/O_2 ashing	40	Ar = 500	330	60	40	O_2 = 500	300	10	1, 5, 8, 10
(f) ALE (plasma–wall interaction)	40	Ar = 500	330	60					5
(g) ALE (gas transition study)	40	Ar = 500	330	60					5

repeatability of etching performances. Thus, it is confirmed that all of our experimental results are repeatable.

III. RESULTS AND DISCUSSION

A. Accuracy evaluation of film thickness measurements

The film thickness was evaluated using SE; however, there was an issue with the measurement accuracy because the film thicknesses were extremely thin. Therefore, the accuracy of the film thickness measurement was evaluated by XPS and TEM. In XPS, the HFC polymer thickness (d_{HFC}) was calculated from the Si (2p) peak area ratio of the SiN. The decrease in Si (2p) intensity, absorbed by the upper HFC polymer, was compared with that of the initial SiN.[22,23] The formula for the HFC polymer thickness is as follows:

$$d_{HFC} = -\lambda_{Si(2p)} \ln\left(\frac{I_{Si(2p)}}{I^{ref}_{Si(2p)}}\right). \quad (1)$$

Here, $\lambda_{Si(2p)}$ is the mean free path of the Si (2p) photoelectrons in the HFC polymer layer. $\lambda_{Si(2p)}$ was set as 2.5 nm in this study. The Si (2p) peak areas of the HFC polymer/SiN sample and initial sample are $I_{Si(2p)}$ and reference of $I_{Si(2p)}$, respectively. Matsui *et al.*[23] reported an assumed escape depth [$\lambda_{Si(2p)}$] of 3 nm. The difference was proposed to result from the composition variations of the HFC polymer. The densification by sputtering in Ar plasma desorption might be the origin of the escape depth decrease in this experiment. After the Ar plasma desorption step, many C–C bonds were generated in the HFC polymer, compared with CH_3F/Ar plasma. Figure 2(a) shows the HFC polymer thickness measured by SE and XPS. Figure 2(b) shows the thicknesses measured by TEM. These figures confirmed that there was a correlation between the HFC polymer film thickness measured by SE, XPS, and TEM. Therefore, the film thickness of the HFC polymer can be measured with high accuracy by SE.

Under the HFC polymer, the modified-SiN layer was generated as shown in Fig. 2(b). This layer was assumed to comprise of mainly Si and N since SE results show that the optical constant of this layer is similar to that of SiN films. This layer could also contain some mixture of C, F, and H. The thickness of the modified-SiN layer is assumed to be defined by the Ar penetration depth and dose in the desorption step. Further study is required to understand the modified layer generation during ALE because the modified layer generation is important to understand the ALE surface reactions.

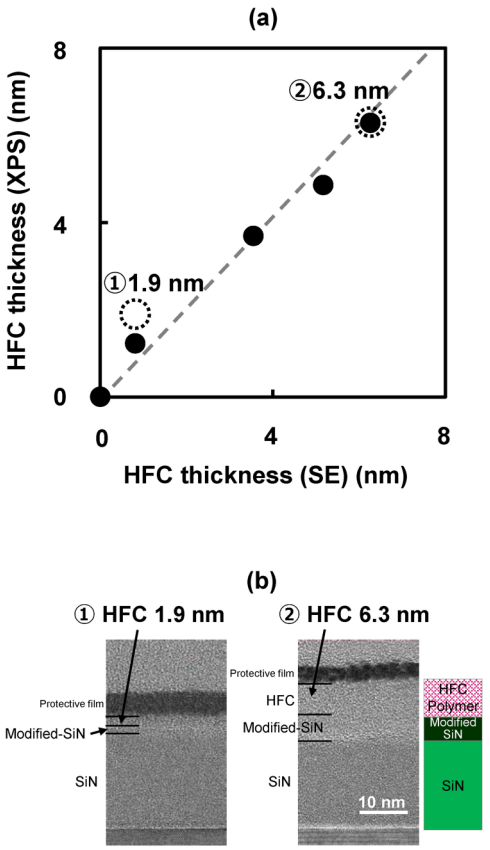

FIG. 2. (a) HFC polymer thicknesses after the adsorption step, measured by XPS vs SE. Dotted circles denote the thicknesses measured by TEM and (b) TEM images (two different process times) [experimental condition; Tables I and II (a)].

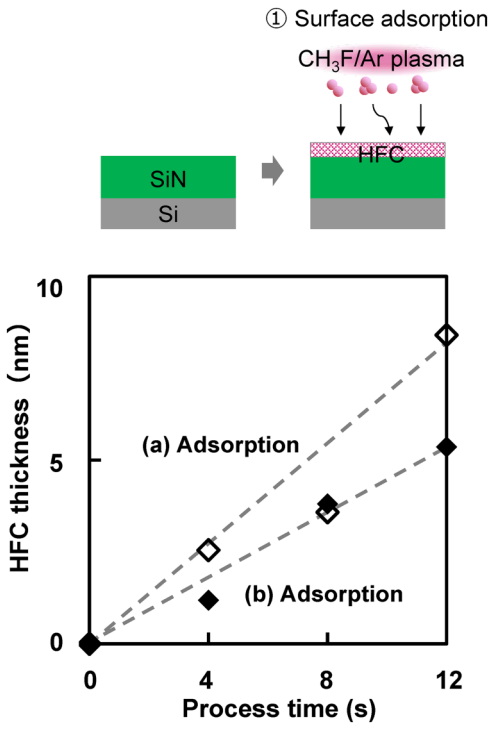

FIG. 3. HFC thicknesses as a function of adsorption process time [experimental condition; Tables I and II (a) and (b)].

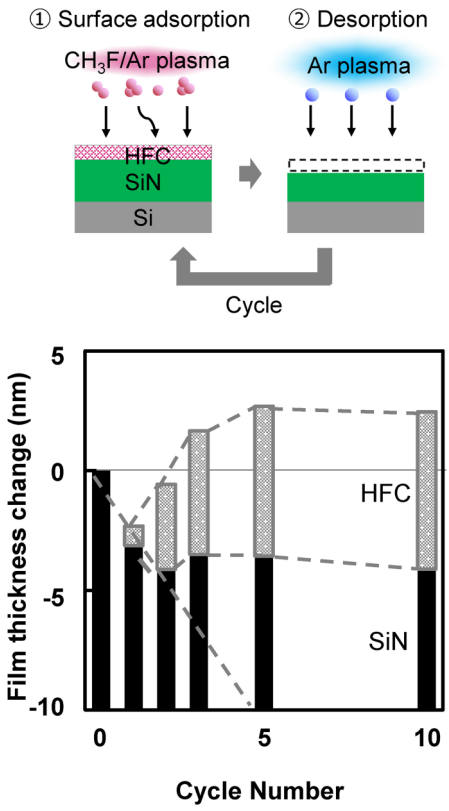

FIG. 4. Cycle number dependence of surface location of HFC and SiN [experimental condition; Tables I and II (c)].

B. SiN ALE etch stop

We studied the optimization of the adsorption step. An HFC film with a thickness of 2 nm was used in a previous study.[11] Thus, the target of the HFC thickness was set to be 2 nm. Figure 3 shows the HFC thicknesses as a function of the process time. The HFC thickness increased linearly with the process time. A 2.6-nm-thick HFC polymer, deposited on SiN, was used as the adsorption step. The desorption time by Ar plasma was set to 10 s. By using this ALE sequence, we studied the cycle number dependence of SiN ALE. The cycle number was changed from 0 to 10. Figure 4 shows the cycle number dependence of the film thickness change of HFC and SiN. The etched amount for one cycle was 0.58 nm. Etching proceeded up to two cycles; however, we observed an etch stop of SiN after ten cycles of ALE, owing to the deposition (>6 nm) of a protective film on the surface. To study the etch-stop phenomena in detail, certain changes to the conditions were also studied (not shown here). In the case of thin HFC adsorption (1.2 nm), an etch stop was also observed regardless of conditions. When the desorption times were changed from 10 to 60 s, we also observed an etch stop. It was concluded that the etch stop is an important issue for stable SiN ALE.

C. Analysis of etch-stop mechanism

To investigate the etch-stop mechanism, the chemical bonding on the SiN surface after one and ten cycles was analyzed by XPS. Figure 5 shows the C (1s) peak which is decomposed into each chemical bond. The binding energies of C–C, C–N, and C–F were 284.8, 286.3, and 287.4 eV, respectively. Figure 5(c) shows the cycle number dependence of the peak area ratio of each bond to the total C (1s) XPS spectra. The ratio of C–C bonds increased with the cycle number of ALE. The bond strength of the C–C bond is 6.4 eV.

It is known that carbon atoms in amorphous carbon films (a-C) hybridize their outermost s and p orbitals of carbon into sp^3 and sp^2 hybrids. Thus, we investigated the sp^3 and sp^2 hybrids by C (1s) spectrum. The binding energy of sp^3 in a-C is 285.2 eV, and the binding energy of sp^2 is 284.4 eV.[24,25] The binding energy of sp^3 and sp^2 was added to Fig. 5(a), and we found that it forms an sp^3 hybrid orbital (similar to diamondlike carbon). Therefore, the HFC polymer, which has many C–C bonds, is difficult to sputter, which results in the etch stop of SiN ALE.

In Fig. 2(b), the modified-SiN layer was generated under the HFC polymer. During air exposure, the oxygen containing layer is also possible to generate under the HFC polymer. Thus, we investigated the C–O and Si–O related peaks in the C (1s) and O (1s) XPS spectra. However, it was found that the oxidation of modified layer under the HFC polymer is of nondetectable level. Thus, we

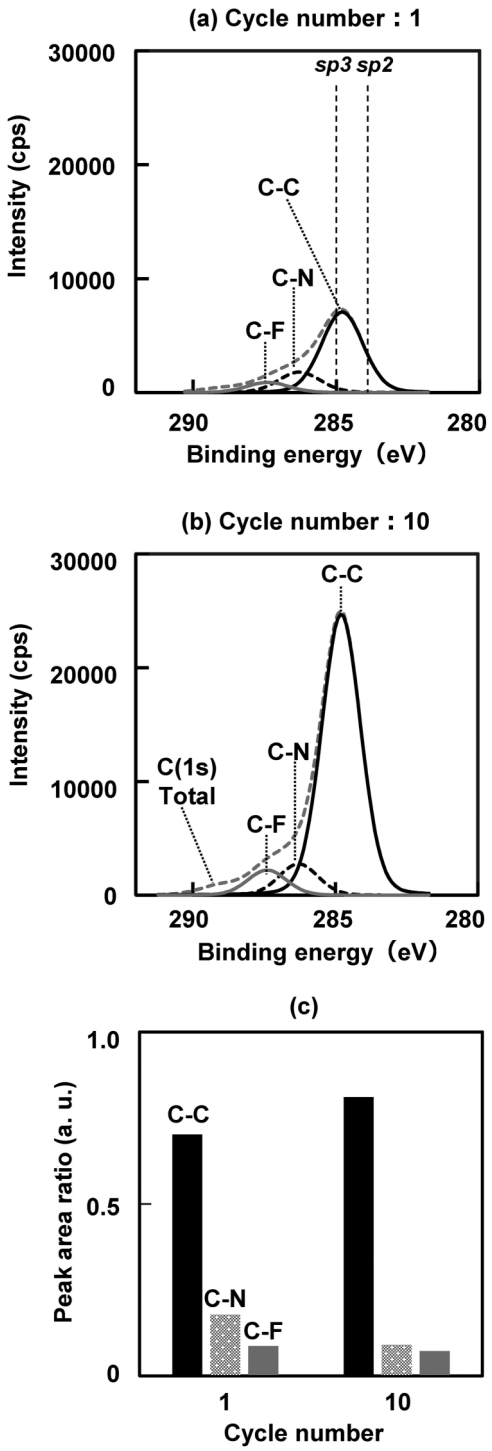

FIG. 5. (a) XPS spectra of C(1s) electron emission on adsorbed HFC layers after one-cycle ALE process and (b) ten-cycle ALE process. The electrons were collected at 90°, and (c) decomposed C–C, C–N, and C–F bond area ratio as a function of cycle number of ALE.

concluded that the modified layer under the HFC polymer is the modified-SiN layer as shown in Fig. 2(b).

Figure 6 shows a schematic of the etch-stop model after adsorption, and after one cycle and ten cycles of ALE. In the adsorption step, the HFC polymer was deposited on SiN. After one cycle of ALE, it was difficult to remove the carbon completely. Strong C–C bonds remained at the surface. After ten cycles, a thick layer of carbon polymer was deposited on the residual carbon. When ions from the plasma pass through the polymer during etching, approximately 200 eV of kinetic energy of the incident ion is reported to be lost in a polymer with a thickness of 1 nm.[26] At 330 eV, which is maximum ion energy of our experimental condition, etching progresses when the polymer thickness is less than 1.5 nm, and etching stops when the film thickness exceeds 1.5 nm from the published results. As shown in Fig. 4, etching progresses through the HFC polymer with a thickness of 0.81 nm at cycle 1. It is expected that etching will proceed when there is energy above 162 eV, in the case that the polymer film thickness is 0.81 nm. However, the ALE ceased after cycle 2 since the polymer thickness of 3.55 nm is much thicker than the threshold thickness of 1.5 nm. Thus, these results are almost consistent with the previous data, published by Tatsumi *et al.* The detailed study of energy loss rate differences in the polymer is a topic of future research, as our study is a rough estimate.

Thus, a thick carbon layer causes an etch stop, and suppression of C deposition is required for stable SiN ALE.

Although we focused on the effect of the C–C bond in the HFC polymer, there are other possibilities that can cause the etch stop of SiN ALE. Another possible reason is that Si–C bonds are formed on the surface.[27–29] As the binding energy of Si–C in the C (1s) photoemission (283.0 eV) is close to the peak position of a strong C–C (284.8 eV) bond, it was difficult to deconvolute the effect of Si–C. As Si–C is generated in the interface between HFC polymer and underlying SiN, the signal of Si–C seems to be under the detectable-level since the upper HFC polymer suppressed the photoelectron from the interface. Further study will be performed related to the Si–C bond by using other techniques.

D. Proposed sequence for stable ALE

For the suppression of excess carbon, physical removal by ion or chemical processes is two possible methods to realize stable ALE. In the case of physical removal using ions, however, longer Ar exposure caused sputtering of the underlayer. Therefore, we focused on the chemical removal. Desorption by O_2/Ar plasma and three-step ALE with O_2 ashing processes were investigated. Although the desorption by O_2 plasma has been reported for SiO_2 ALE,[30] SiN ALE with an O_2-based process has not been reported (to the best of our knowledge).

To investigate the effect of oxygen, the desorption step with O_2/Ar plasma was examined. The desorption time was 60 s and 0–10 cycles of ALE were performed. Figure 7 shows the etched amount per cycle (EPC) as a function of cycle number in the case of a desorption step by O_2/Ar plasma. The EPC was 0.89 nm/cycle. SiN ALE proceeded continuously by the O_2/Ar plasma desorption step. The HFC polymer deposition was suppressed by O_2 addition. Next, we examined a three-step ALE with O_2 ashing. The desorption and ashing times

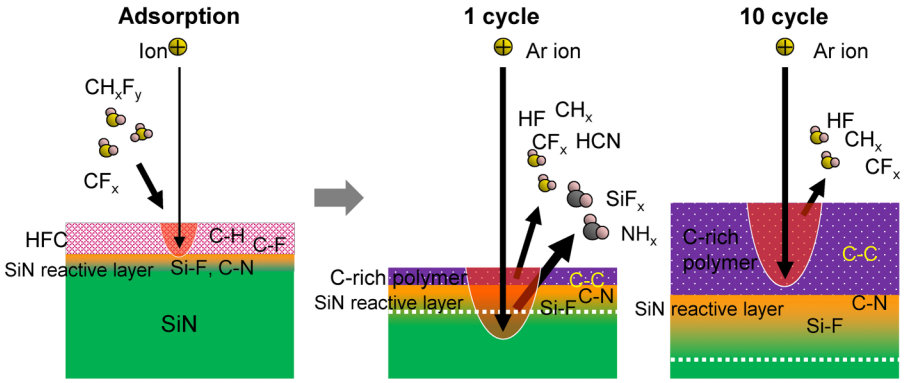

FIG. 6. Schematic models after the adsorption step, one-cycle ALE, and ten-cycle ALE.

were 60 and 10 s, and 0–10 cycles of ALE were performed. Figure 8 shows the EPC as a function of cycle number in the case of the three-step ALE with O_2 ashing. The EPC was 1.52 nm/cycle. Therefore, the O_2 ashing step effectively removed the HFC polymer.

The EPC of the three-step ALE was much higher than that of O_2/Ar desorption. We discuss the amount of fluorine during ALE because the EPC of SiN is strongly related to the amount of fluorine on the SiN surface. The high EPC of the three-step ALE was caused by the presence of abundant fluorine atoms in the HFC during Ar desorption, compared with O_2/Ar desorption. In the case of the three-step ALE with O_2 ashing, the HFC film remained in the desorption step. This caused the high EPC of SiN ALE. In

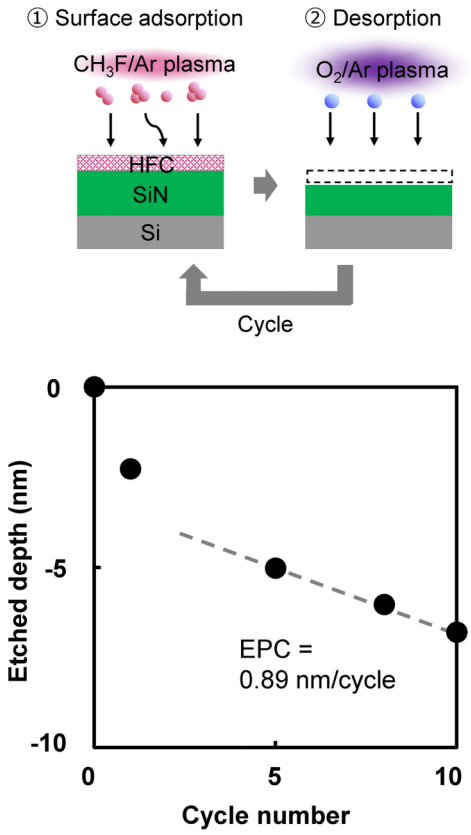

FIG. 7. Etched depths as a function of cycle number in the case of a desorption step by O_2/Ar plasma [experimental condition; Tables I and II (d)].

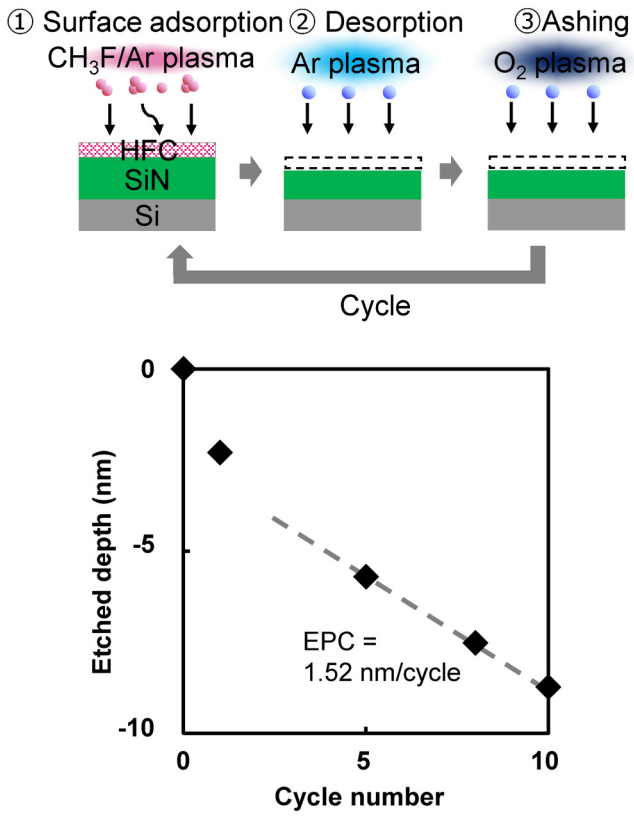

FIG. 8. Etched depths as a function of cycle number in the case of three-step ALE with subsequent O_2 ashing [experimental condition; Tables I and II (e)].

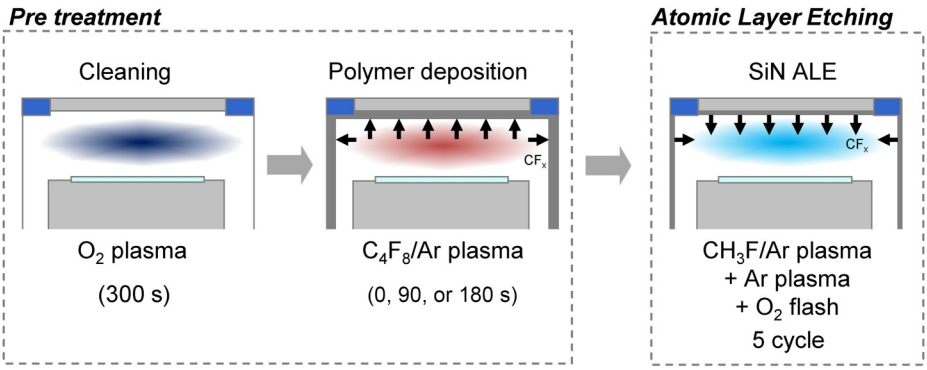

FIG. 9. Schematic of the experiment to investigate the plasma–wall interactions. The chamber conditions were intentionally varied.

the case of O_2/Ar desorption, the HFC was removed simultaneously during the desorption step. This caused the low EPC. As the three-step ALE is appropriate for device manufacturing, we used three-step ALE in the subsequent investigations. We also confirmed that EPC of first and second cycles was higher than that for the other cycles. Impurities from the plasma, which were implanted in the SiN surface during ALE cycles, modified the SiN surface to cause the decrease of the SiN EPC with additional cycles.

E. SiN ALE fluctuation

A key parameter of SiN ALE is the amount of fluorine, which dominantly contributes to SiN etching. In addition, the amount of carbon affects the EPC fluctuation in ALE. Excess carbon causes the etch stop and less carbon may cause the low EPC. As the amounts of fluorine and carbon are important, the effect of density fluctuations by C/F species was studied.

As the plasma–wall interactions were reported to cause the C/F density fluctuation,[21,22] the chamber wall condition was intentionally changed. We performed the O_2 cleaning and polymer deposition with C_4F_8/Ar plasma. The deposition time was 0, 90, or 180 s. Then, we performed the SiN ALE for five cycles using the same conditions (Fig. 9). Figure 10 shows the etched depth uniformity differences with and without chamber wall polymer deposition. The etched depth at the wafer edge increased drastically. We proposed that the desorbed species from the wall surface affected the etch rate fluctuation. Because CF_2, measured by appearance mass spectroscopy, is reported to be desorbed from the deposited polymer with Ar ion injection,[31] desorbed CF_2 enhance the EPC at the wafer edge during Ar desorption. When we investigated the optical emission spectra of CF_2 ($\lambda = 262.5$ nm) during the Ar desorption step (not shown here), a clear increase of the CF_2 radical was detected with the chamber wall deposited conditions. In the case of O_2 cleaning, however, the CF_2 desorption from the chamber wall was suppressed. We concluded that the chamber wall condition is important for stable ALE processes. Under the condition that there was no deposition on the reactor wall, the etched depth uniformity across the wafer was poor. However, it can be improved by optimizing the Ar desorption process.

Next, we studied the effect of residual gases from the previous step. A mixture of residual gas from the previous step might cause C/F density fluctuation. We changed the gas transition time before the Ar desorption step from 20 to 1 s (Fig. 11). Figure 12 shows the etched depth uniformity differences at gas transition times of 1 and 20 s as a function of wafer coordinate. There was almost no difference in etched depth after ALE (adsorption and desorption) with

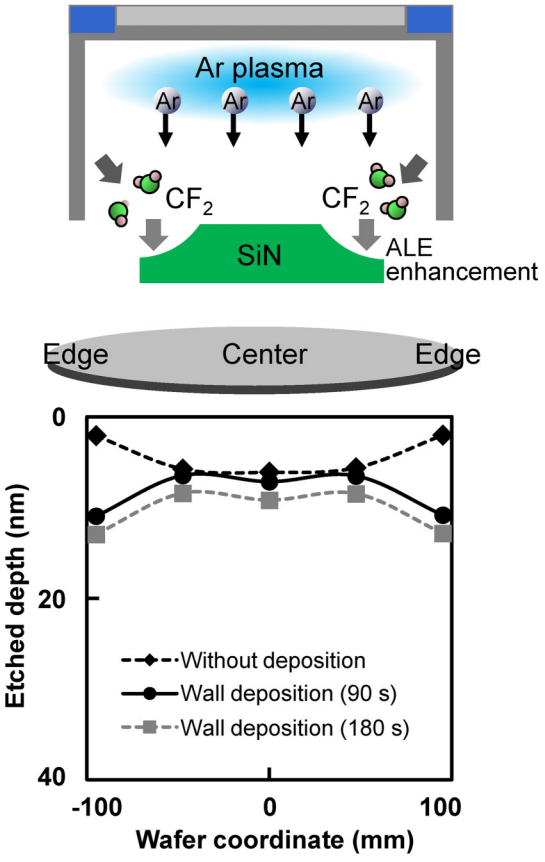

FIG. 10. Etched depth uniformity differences with and without polymer deposition on the chamber wall [experimental condition; Tables I and II (f)].

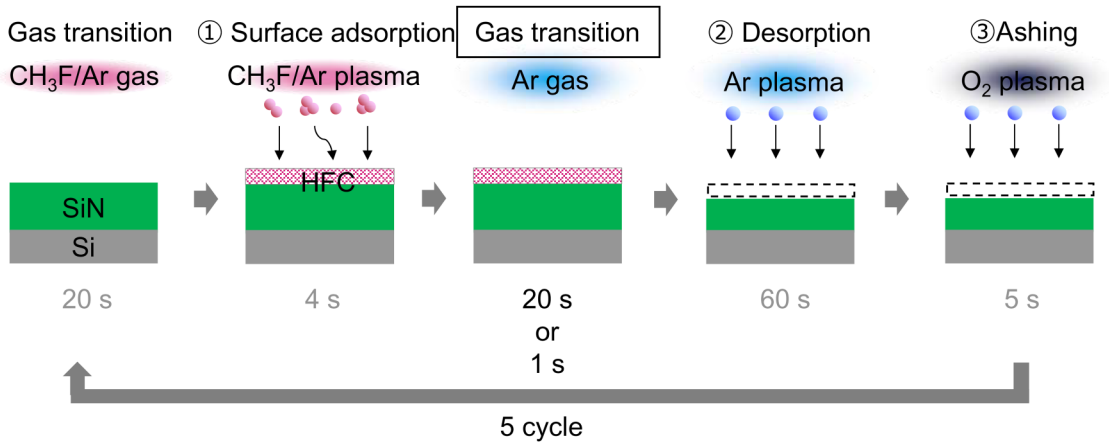

FIG. 11. Schematic illustration of experiments for gas transition time dependence.

gas transition times of 20 and 1 s. We found that residual gases have almost no impact on ALE because the gas residence time under the experimental condition was 63 ms, which is much shorter than the gas transition time (1 s). Therefore, the transition time has a negligible effect on the etched depth fluctuation.

We proposed the fluctuation model of SiN ALE caused by the plasma–wall interaction. CF_2 desorption from the chamber wall caused the ALE enhancement. Therefore, we need to clean the chamber before ALE. We found that control of fluorine and carbon amounts is critical for stable SiN ALE.

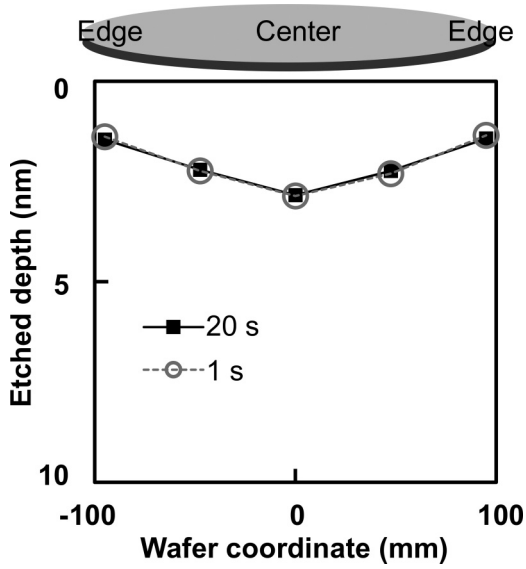

FIG. 12. Etched depth uniformities as a function of wafer coordinate with different gas transition time (20 vs. 1 s) [experimental condition; Tables I and II (g)].

IV. SUMMARY AND CONCLUSIONS

ALE has been studied extensively for surface reactions, and thus, little has been reported about the fluctuation of ALE performances in device fabrication. In this study, we investigated SiN ALE with process optimization of the adsorption and desorption steps, and we focus on the cycle number dependence of EPC fluctuation of ALE. We also studied the ALE performance variation caused by the chamber wall conditions. Our findings are as follows.

(1) Excess polymer deposition, which originates from residual carbon after desorption step, causes the etch stop of SiN ALE. The reason of residual carbon is that the HFC polymer, which has many C–C bonds, is difficult to sputter. Thus, a thick carbon layer causes an etch stop, and suppression of C deposition is required for stable SiN ALE.
(2) Addition of O_2 to the desorption step or a three-step O_2 ashing process can suppress C deposition and realize stable ALE. The high EPC of the three-step ALE was caused by the presence of abundant fluorine atoms in the HFC during Ar desorption, compared with O_2/Ar desorption. Hence, the three-step ALE is appropriate for device manufacturing.
(3) CF_x desorption from the chamber wall causes etch enhancement of ALE. The desorbed CF_2 enhance the EPC at the wafer edge during Ar desorption. We found that control of fluorine and carbon amounts is critical for stable SiN ALE.

To realize stable SiN ALE, it is necessary to keep the same surface conditions in every cycle. It is also important to control the influence of desorbed species from the chamber components. As the etching selectivity to other materials is critical for semiconductor device manufacturing, further study related to the selectivity to mask and/or underlying materials is strongly required in the near future.

REFERENCES

[1]K. J. Kanarik, T. Lill, E. A. Hudson, S. Sriraman, S. Tan, J. Marks, V. Vahedi, and R. A. Gottscho, J. Vac. Sci. Technol. A **33**, 020802 (2015).
[2]K. J. Kanarik *et al.*, J. Vac. Sci. Technol. A **35**, 05C302 (2017).
[3]K. J. Kanarik, S. Tan, and R. A. Gottscho, J. Phys. Chem. Lett. **9**, 4814 (2018).
[4]Y. Horiike, T. Tanaka, M. Nakano, S. Iseda, H. Sakaue, A. Nagata, H. Shindo, S. Miyazaki, and M. Hirose, J. Vac. Sci. Technol. A **8**, 1844 (1990).
[5]D. Metzler, R. L. Bruce, S. Engelmann, E. A. Joseph, and G. S. Oehrlein, J. Vac. Sci. Technol. A **32**, 020603 (2014).
[6]D. Metzler, C. Li, S. Engelmann, R. L. Bruce, E. A. Joseph, and G. S. Oehrlein, J. Vac. Sci. Technol. A **34**, 01B101 (2016).
[7]D. Metzler *et al.*, J. Vac. Sci. Technol. A **34**, 01B102 (2016).
[8]K.-Y. Lin, C. Li, S. Engelmann, R. L. Bruce, E. A. Joseph, D. Metzler, and G. S. Oehrlein, J. Vac. Sci. Technol. A **36**, 040601 (2018).
[9]M. Honda, T. Katsunuma, M. Tabata, A. Tsuji, T. Oishi, T. Hisamatsu, S. Ogawa, and Y. Kihara, J. Phys. D Appl. Phys. **50**, 234002 (2017).
[10]C. Li, D. Metzler, C. S. Lai, E. A. Hudson, and G. S. Oehrlein, J. Vac. Sci. Technol. A **34**, 041307 (2016).
[11]Y. Ishii, K. Okuma, T. Saldana, K. Maeda, N. Negishi, and J. Manos, Jpn. J. Appl. Phys. **56**, 06HB07 (2017).
[12]A. Hirata, M. Fukasawa, K. Kugimiya, K. Nagaoka, K. Karahashi, S. Hamaguchi, and H. Iwamoto, Jpn. J. Appl. Phys. **59**, SJJC01 (2020).
[13]N. Posseme, V. Ah-Leung, O. Pollet, C. Arvet, and M. Garcia-Barros, J. Vac. Sci. Technol. A **34**, 061301 (2016).
[14]S. D. Sherpa and A. Ranjan, J. Vac. Sci. Technol. A **35**, 01A102 (2017).
[15]K. Nakane, R. H. J. Vervuurt, T. Tsutsumi, N. Kobayashi, and M. Hori, ACS Appl. Mater. Interfaces **11**, 37263 (2019).
[16]A. Hirata, M. Fukasawa, T. Shigetoshi, M. Okamoto, K. Nagahata, H. Li, K. Karahashi, S. Hamaguchi, and T. Tatsumi, Jpn. J. Appl. Phys. **56**, 06HD02 (2017).
[17]A. Hirata, M. Fukasawa, K. Nagahata, H. Li, K. Karahashi, S. Hamaguchi, and T. Tatsumi, Jpn. J. Appl. Phys. **57**, 06JB02 (2018).
[18]T. Sasaki, K. Matsuda, M. Omura, I. Sakai, and H. Hayashi, Jpn. J. Appl. Phys. **54**, 06GB03 (2015).
[19]N. Marchack, J. Innocent-Dolor, M. Hopstaken, and S. Engelmann, J. Vac. Sci. Technol. A **38**, 022609 (2020).
[20]M. Schaepkens, R. C. M. Bosch, T. E. F. M. Standaert, G. S. Oehrlein, and J. M. Cook, J. Vac. Sci. Technol. A **16**, 2099 (1998).
[21]M. Fukasawa, A. Kawashima, N. Kuboi, H. Takagi, Y. Tanaka, H. Sakayori, K. Oshima, K. Nagahata, and T. Tatsumi, Jpn. J. Appl. Phys. **48**, 08HC01 (2009).
[22]T. E. F. M. Standaert, M. Schaepkens, N. R. Rueger, P. G. M. Sebel, G. S. Oehrlein, and J. M. Cook, J. Vac. Sci. Technol. A **16**, 239 (1998).
[23]M. Matsui, F. Uchida, M. Kojima, T. Tokunaga, F. Yano, and M. Hasegawa, J. Vac. Sci. Technol. A **20**, 117 (2002).
[24]J. Díaz, G. Paolicelli, S. Ferrer, and F. Comin, Phys. Rev. B **54**, 8064 (1996).
[25]Y. Mizokawa, T. Miyasato, S. Nakamura, K. M. Geib, and C. W. Wilmsen, J. Vac. Sci. Technol. A **5**, 2809 (1987).
[26]T. Tatsumi, M. Matsui, M. Okigawa, and M. Sekine, J. Vac. Sci. Technol. B **18**, 1897 (2000).
[27]G. J. Coyle and G. S. Oehrlein, Appl. Phys. Lett. **47**, 604 (1985).
[28]R. Blanc, F. Leverd, T. David, and O. Joubert, J. Vac. Sci. Technol. B **31**, 051801 (2013).
[29]R. Blanc, C. Jenny, S. Lagrasta, F. Leverd, and O. Joubert, J. Vac. Sci. Technol. B **32**, 021806 (2014).
[30]T. Tsutsumi, H. Kondo, M. Hori, M. Zaitsu, A. Kobayashi, T. Nozawa, and N. Kobayashi, J. Vac. Sci. Technol. A **35**, 01A103 (2017).
[31]K. Nakamura, K. Kumagai, T. Tatsumi, and K. Oshima, in *Proceedings of the International Symposium on Dry Process*, Jeju, Korea, 28 November 2005 (DPS, Korea, 2005), p. 99.